



Explicit finite element analysis and experimental verification of a sliding lead rubber bearing^{*}

Yi-feng WU^{†1}, Hao WANG^{†‡1}, Ai-qun LI^{1,2}, Dong-ming FENG³, Ben SHA¹, Yu-ping ZHANG¹

(¹School of Civil Engineering, Southeast University, Nanjing 210096, China)

(²Beijing Advanced Innovation Center for Future Urban Design, Beijing University of Civil Engineering and Architecture, Beijing 100044, China)

(³Department of Civil Engineering and Engineering Mechanics, Columbia University, New York, NY 10027, USA)

[†]E-mail: wyf.07010701@163.com; wanghao1980@seu.edu.cn

Received Apr. 9, 2016; Revision accepted Aug. 31, 2016; Crosschecked Apr. 14, 2017

Abstract: Based on the explicit finite element (FE) software ANSYS/LS-DYNA, the FE model for a sliding lead rubber bearing (SLRB) is developed. The design parameters of the laminated steel, including thickness, density, and Young's modulus, are modified to greatly enlarge the time step size of the model. Three types of contact relations in ANSYS/LS-DYNA are employed to analyze all the contact relations existing in the bearing. Then numerical simulations of the compression tests and a series of correlation tests on compression-shear properties for the bearing are conducted, and the numerical results are further verified by experimental and theoretical ones. Results show that the developed FE model is capable of reproducing the vertical stiffness and the particular hysteresis behavior of the bearing. The shear stresses of the intermediate rubber layer obtained from the numerical simulation agree well with the theoretical results. Moreover, it is observed from the numerical simulation that the lead cylinder undergoes plastic deformation even if no additional lateral load is applied, and an extremely large plastic deformation when a shear displacement of 115 mm is applied. Furthermore, compared with the implicit analysis, the computational cost of the explicit analysis is much more acceptable. Therefore, it can be concluded that the proposed modeling method for the SLRB is accurate and practical.

Key words: Explicit analysis; Sliding lead rubber bearing (SLRB); Time step size; Contact relations; Numerical simulation; Experimental verification

<http://dx.doi.org/10.1631/jzus.A1600302>

CLC number: U448.21

1 Introduction

Since the invention and application of laminated rubber bearings, the technology has been widely developed. The basic aim is to extend the natural vibration period and to increase the damping ratio of

structures. In recent decades, seismic isolation techniques have been promoted to improve seismic performance for structures, such as buildings, bridges, and nuclear power plants, in developed countries. For example, Warn and Ryan (2012) reviewed the historic development and research needs of seismic isolation for buildings. Basu *et al.* (2014) reviewed recent research and applications of structural control technology, including passive, semi-active, and active control systems, and the investigation of their performance in civil engineering across Europe. Medel-Vera and Ji (2015) provided a systematic review of the seismic protection systems of nuclear power plants, and Perotti *et al.* (2013) proposed a numerical

[‡] Corresponding author

^{*} Project supported by the National Natural Science Foundation of China (Nos. 51278104, 51578151, and 51438002) and the Program for New Century Excellent Talents in University of Ministry of Education, China (No. NCET-13-0128)

 ORCID: Yi-feng WU, <http://orcid.org/0000-0002-6932-2329>; Hao WANG, <http://orcid.org/0000-0002-1187-0824>

© Zhejiang University and Springer-Verlag Berlin Heidelberg 2017

procedure to compute the seismic fragility function of seismic isolation in nuclear power plants. Meanwhile, some specialized standards and guidelines were compiled for engineering designers to follow (Imbsen, 2007). In China, because of recent severe earthquakes, more efforts have been devoted to improving structural seismic performance. Pan *et al.* (2012) presented an overall review of the representative applications of seismic isolation and energy dissipation structures in China. As an effective way to reduce seismic responses of structures, seismic isolation devices have been extensively studied during the past few decades. For example, Tyler and Robinson (1984) focused on the mechanical characteristics of lead rubber bearings that were subjected to high strains; Hwang *et al.* (1996) proposed a refined model for bi-linear hysteretic bearings; Ryan *et al.* (2004) studied particular effects of axial load on rubber bearings by experiment; Abe *et al.* (2004a; 2004b) studied the cyclic behavior of three types of laminated rubber bearings under a multi-axial loading state by experiment and numerical simulations; Warn *et al.* (2007) investigated the influence of lateral displacement on the vertical stiffness of elastomeric and lead-rubber bearings. The stability of seismic isolation bearings was studied and a mechanistic model was proposed for simulating the critical behavior of bearings (Weisman and Warn, 2012; Han and Warn, 2014). Kelly and Marsico (2013) proposed an analytical formulation to predict tension buckling in rubber bearings affected by cavitation. de Mari *et al.* (2015) introduced a reduced-order coupled bidirectional numerical model to characterize the mechanical properties of a novel Roll-*N*-Cage isolator and applied that isolator to a benchmark cable-stayed bridge to assess its seismic mitigation effect. As for numerical simulations of bearings, Takayama *et al.* (1992) used the finite element (FE) method to obtain the load-deformation relationship of laminated rubber bearings; Ali and Abdel-Ghaffar (1995) elaborated on the modeling of rubber and lead passive-control bearings for seismic analyses; Imbimbo and de Luca (1998) used ABAQUS to investigate the influence of the shape factor on the stress distribution and stress concentration of a laminated rubber bearing; Dou-doumis *et al.* (2005) performed the quasi-static analysis of lead rubber bearings by ADINA; Yoshida *et al.* (2004) presented a novel constitutive model for

high damping materials and employed it in the simulation of high damping rubber bearings; Amin *et al.* (2002; 2006a; 2006b) made thorough studies of the numerical modeling and experimental verification of high damping rubber bearings; Nguyen and Tassoulas (2010) analyzed the effects of shear direction on bearing behavior by ABAQUS; Kalpakidis *et al.* (2010) considered the influence of increase of temperature on the mechanical properties of lead rubber bearings; Wang *et al.* (2014) used LS-DYNA to realize the analytical simulations of elastomeric bridge bearings. For all these studies, bearings are discretized into solid elements. However, in the numerical simulation of seismic isolation structures, rubber bearings usually are simplified to be special elements or materials, like COMBIN40 in ANSYS and *MAT_SPRING in LS-DYNA, which characterize mainly the compression and shear properties of bearings. For example, Roussis *et al.* (2003) presented an evaluation of the design of a seismic isolation system for a viaduct and an assessment of its performance in the Duzce earthquake; Domaneschi (2012) employed the phenomenological Bouc-Wen model to control in real time the hysteresis of semi-active control systems in seismic isolated structures; Gur *et al.* (2014) compared seismic responses of buildings isolated using a shape-memory alloy rubber bearing and a lead rubber bearing; Eröz and DesRoches (2013) conducted a comparative assessment of a friction pendulum system versus a lead rubber bearing in typical multi-span bridges.

Most current numerical simulations of bearings using solid elements are based on implicit FE programs, in which case iterative calculations usually encounter convergence problems when bearings undergo large deformations, especially when the hyperelastic model for rubber is employed in the FE model. Besides, effective simulation of the complicated contact relations existing in bearings and the reduction of the computational cost are two other challenges. Recently, Ohsaki *et al.* (2009; 2015) carried out FE analyses for a building frame equipped with laminated rubber bearings by a parallel FE analysis software package ADVENTURECluster (Miyamura *et al.*, 2015), in which the whole structure was discretized into solid elements with more than three million degrees of freedom, and the numerical results were verified using the test results from a

full-scale shake-table. Despite all this progress, the study of fine numerical simulations for rubber bearings and structures is still needed.

In this study, to realize the numerical simulation of a sliding lead rubber bearing (SLRB) (Xing *et al.*, 2012), the FE model of the bearing, which is discretized into hexahedral solid elements, is developed using the explicit FE software ANSYS/LS-DYNA. Then numerical simulations of the compression tests and a series of correlation tests on compression-shear properties for the bearing are conducted, and the results obtained are validated against experimental and theoretical results. As a first step for further studies on seismic isolation bridges equipped with SLRBs, we aim to present an accurate and practical method for the modeling of bearings.

2 Configuration and working principle of the sliding lead rubber bearing

2.1 Configuration

Fig. 1 shows the design drawing of the SLRB. It consists of two parts in the vertical direction, i.e., the upper sliding device (Fig. 2a) and the lower lead rubber bearing (LRB). The sliding device, comprised of the top connection plate, stainless steel plate, and baffle, is placed on top of the Teflon plate, which is

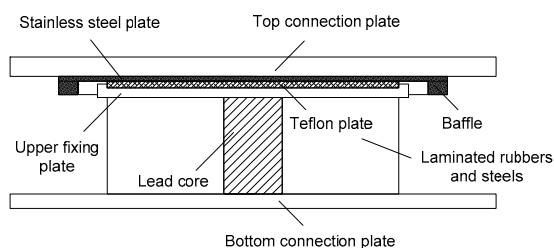


Fig. 1 Design drawing of the sliding lead rubber bearing (SLRB)



Fig. 2 Model of the sliding lead rubber bearing (a) Sliding device and Teflon plate; (b) A specimen

embedded tightly in the upper fixing plate of the LRB. The diameter of the LRB is 300 mm. The slide limit between the baffle and the upper fixing plate of the LRB is 15 mm. The baffle is made up of four steel blocks, which are bolted to the stainless steel plate and the top connection plate. Other design parameters of the SLRB are listed in Table 1, and a specimen of the SLRB is shown in Fig. 2b.

Table 1 Mechanical parameters of the sliding lead rubber bearing (SLRB)

Parameter	Value
Shear modulus of rubber (MPa)	0.392
Effective diameter (mm)	300
Diameter of the lead core (mm)	60
Thickness of the laminated steel (mm)	1.5
Number of layers of the laminated steel	17
Thickness of the rubber (mm)	3.39
Number of layers of the rubber	18
First shape coefficient	22.12
Second shape coefficient	4.92
Height of the SLRB (mm)	106.5

2.2 Working principle of the sliding lead rubber bearing

The SLRB integrates the features of sliding bearings and lead rubber bearings. It can protect bridges by adapting to deformations caused by temperature, vehicle impacts, and concrete creep under normal conditions, and has a seismic isolation function during an earthquake. The working principle of the SLRB can be summarized as follows (Xing *et al.*, 2012). When the lower LRB initially generates a tiny displacement, the shear force is transmitted directly to the upper sliding device. As the shear displacement increases, the upper sliding device will work and glide on the Teflon plate if the shear force of the LRB exceeds the maximum static friction force of the Teflon-stainless steel interface. The upper fixing plate will hit the baffle after the relative sliding displacement of the upper device reaches the design slide limit, and the LRB begins to show typical bi-linear hysteretic dissipation characteristics. The above procedures can be summarized as ‘slide-isolation’; namely, the upper device slides first and then both the two parts of the SLRB act as a seismic isolation entirety. During the unloading stage, LRB first recovers

vertically after reaching the maximum displacement, and then the next ‘slide-isolation’ circulation starts.

3 Finite element model of the sliding lead rubber bearing

ANSYS/LS-DYNA is a widely used explicit FE program package. It contains more than 200 material models and an advanced contact algorithm, making it capable of solving complicated problems in material nonlinearity, geometrical nonlinearity, and contact nonlinearity. Here, the ANSYS/LS-DYNA code is used to develop the FE model of the SLRB. The pre-processing of the model is done using the ANSYS Parametric Design Language (APDL) and an executable input file of the model is achieved. Then modifications of material models and contact relations are required in the file before the file is submitted to the LS-DYNA processor. The developed FE model of the SLRB is illustrated in Fig. 3, which includes 14 128 solid hexahedron 8-node elements (Solid 163) and 17 164 nodes.

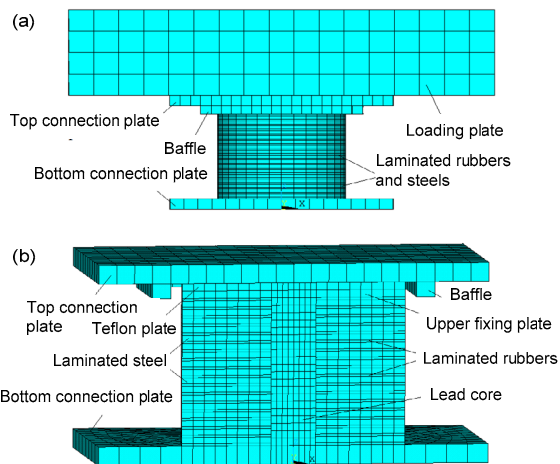


Fig. 3 Finite element model of the sliding lead rubber bearing

(a) Total analytical model; (b) Semi-model of the sliding lead rubber bearing

Obvious differences can be found between the original configuration of the SLRB and the FE model. Besides, certain design parameters of the materials need to be modified to enable the implementation of the analysis.

3.1 Simplification and modification for the finite element model

1. In dynamic explicit FE analyses, reduced integral elements are usually preferred to achieve reasonable runtime which, however, may cause undesired hourglass models in some cases, especially in the case of poor mesh or when subjected to concentrated forces. To avoid this problem, both rubber layers and steel shims are modeled by full integration S/R solid elements (defined by the keyword *ELEMENT_SOLID) in this study.

2. In the manufacturing process of the SLRB, rubbers and steels are glued together by vulcanization. Adjacent steels are connected tightly by bolt. All of these relations are assumed to be fully bonded and simulated by common nodes in the FE model of the SLRB.

3. As illustrated in Figs. 1 and 2a, part of the Teflon plate is embedded in the upper fixing plate, while in the FE model, the Teflon plate is modified to be on the top of the upper fixing plate for convenience. The stainless steel is removed in the FE model and the top connection plate slides directly on the Teflon plate. In addition, the outside rubber covering of the lower LRB is neglected due to the computational cost since its thickness is very small.

3.2 Time step size of the finite element model

One major difference between the configuration and the FE model of the SLRB is the thickness of the laminated steels. As listed in Table 1, their actual thickness is 1.5 mm and it is smaller than that of the rubber, while in the FE model, the thickness of the laminated steels is magnified several times and it is larger than that of the rubber (Fig. 3b).

In explicit FE analyses, the computational cost of a project is negatively correlated with the time step size (Δt) in each cycle, and Δt is obtained by taking the minimum value over all elements (Hallquist, 2014):

$$\Delta t = \alpha \cdot \min \{ \Delta t_{e_1}, \Delta t_{e_2}, \dots, \Delta t_{e_i}, \dots, \Delta t_{e_n} \}, \quad (1)$$

where n is the number of elements and Δt_{e_i} is the critical time step size (CTSS) of the i th element. The scale factor α is typically set to a value of 0.90 for stability reasons.

For beam and truss elements, the CTSS is given by

$$\Delta t_e = \frac{L}{c}, \quad (2)$$

where L is the length of the element and c the wave speed of relative materials satisfying

$$c = \sqrt{\frac{E}{\rho}}, \quad (3)$$

with E Young's modulus and ρ the density.

The influence of these three parameters (L , E , and ρ) on the CTSS of solid elements is similar to that on the CTSS of beam elements, meaning that the CTSS has positive correlation with the size and density of elements, and a negative one with Young's modulus (Hallquist, 2014).

According to Eqs. (1)–(3), the time step size Δt of the SLRB model is determined primarily by an element of the laminated steels in the case of no modifications, and the CTSS of the element is much smaller than others' since the Young's modulus of steels is the largest and the thickness of the laminated steels is the smallest. In this case, the computational cost will be out of control.

Under these circumstances, it is necessary to activate the in-built mass scaling (or density scaling) technique supplied by ANSYS/LS-DYNA to enlarge the CTSS of certain elements. However, as shown in Eqs. (2) and (3), the CTSS is proportional to the square root of the density, in which case CTSS will be magnified by approximately 10 times when magnifying the density of beam elements by 100. Nonetheless, it will be more efficient by magnifying the length of elements since Δt_e is proportional to the length of elements.

On the other hand, taking circular LRBs as an example, the vertical stiffness can be calculated by Eq. (4) (SAC, 2006), and the horizontal bi-linear mechanical properties can be defined by Eqs. (5)–(8) (Sugita *et al.*, 1994):

$$K_v = \frac{45\pi G d_e^3}{16n t_e^2}, \quad (4)$$

$$K_u = 6.5K_d, \quad (5)$$

$$K_d = \frac{F - Q_d}{u}, \quad (6)$$

$$F = A_R G \gamma + A_p q, \quad (7)$$

$$Q_d = A_p q_0, \quad (8)$$

where K_v is the vertical stiffness, G is the shear modulus of rubber, d_e is the diameter of the laminated steel, n is the number of rubber layers, t_e is the thickness of the rubber layers, K_u and K_d are the pre- and post-yield stiffnesses, respectively, A_R and A_p are the cross sectional areas of the rubber and the lead core, respectively, γ is the shear strain of rubber, F is the resilience of the bearing, q is the cross section shear stress of the lead core which is a function of the shear strain γ , q_0 is the shear stress of the lead core when the shear strain of it is zero, Q_d is the characteristic strength of the bearing, and u represents the target displacement of the bearing.

According to Eqs. (4)–(8), the vertical stiffness and the horizontal mechanical properties of LRBs are theoretically irrelevant to the thickness, Young's modulus, and density of the laminated steels. Therefore, the mass scaling technology and the modifications of the thickness, as well as Young's modulus, of steels are all employed to magnify the CTSS of laminated steels to a considerable degree. The thickness of the laminated steels is modified from 1.5 mm to 8 mm, the Young's modulus of steel is modified from 210 GPa to be the same as that of lead, i.e., 16.46 GPa, and the density will be magnified automatically by the software. All of these modifications will inevitably lead to errors. However, as verified above, these errors are practically negligible since the mechanical properties of rubber bearings are determined mostly by the design parameters of the rubber rather than those of the steel.

In the FE model, other constitutive parameters are set to be normal ones. The steel material has a Poisson's ratio of 0.30, and is assumed a bi-linear elastoplastic constitutive law with 10% strain hardening ratio and a von Mises yield criterion with $\sigma_y = 235$ MPa (*MAT_PLASTIC_KINEMATIC). The lead core is assumed to have a Young's modulus of 16.46 GPa, a Poisson's ratio of 0.44, and ideal elastoplastic constitutive law with its yield stress 16 MPa (*MAT_PLASTIC_KINEMATIC). For the rubber layers, a hyperelastic material law, Mooney-Rivlin

model (*MAT_MOONEYRIVLIN_RUBBER), is employed, and three material constants in this model are set as $C_1=0.1633$ MPa, $C_2=0.03267$ MPa, and Poisson's ratio 0.4999. The Teflon plate is assumed to be an elastic material (*MAT_ELASTIC) with a Young's modulus of 300 MPa and a Poisson's ratio of 0.4.

With all the aforementioned modifications for the FE model of the SLRB, the time step size Δt of the model is increased from 2.4×10^{-7} s to 3.5×10^{-6} s, which means that the computation time is reduced by about 93.1% and the computational cost is significantly reduced.

3.3 Contact relations in the finite element model

In the SLRB, the stainless steel plate is supposed to slide on the Teflon plate, and the baffle is used to control the displacement of the sliding device. The lead core is hooped tightly by its surrounding rubbers and steels. All of these interactions are simulated by *CONTACT series in ANSYS/LS-DYNA. The common keyword *CONTACT AUTOMATIC SURFACE TO SURFACE SMOOTH is used to simulate the possible contact between the upper fixing plate and the baffle, in which the friction coefficient is set to be 0.04. However, this keyword cannot simulate the sliding contact between the Teflon plate and the top connection plate very well, because the mesh grid of the slave elements will block the horizontal displacement of the intrusive master nodes. Instead, the keyword *CONTACT ONE WAY AUTOMATIC SURFACE TO SURFACE SMOOTH is employed to simulate the interactions since it does not check whether the master nodes penetrate into the slave mesh grid, and the friction coefficient in this keyword is set as 0.055. In addition, to simulate the actual loading conditions of the SLRB, a loading plate is placed on the top of the bearing. The size of the loading plate is 1000 mm×1000 mm×200 mm, and the material of the plate is steel with Young's modulus 210 GPa and Poisson's ratio 0.3 (*MAT_ELASTIC). The contact between the loading plate and the bearing is also analyzed by the keyword *CONTACT AUTOMATIC SURFACE TO SURFACE SMOOTH with a friction coefficient of 0.4. Besides, the contact caused by an interference fit between the lead core and its surrounding items, including laminated rubbers, steels, bottom connection

plate, and upper fixing plate, can be well simulated by the keyword *CONTACT TIED SURFACE TO SURFACE SMOOTH, and the friction coefficient is also set to be 0.4.

4 Loading equipment and procedures

As illustrated in Fig. 2b, a specimen of the SLRB was developed based on the parameters in Table 1. The vertical compression and nonlinear shear performances of the bearing were experimentally investigated. The tests were carried out on a large press-shear machine (PSM) (Fig. 4) in Huazhong University of Science and Technology, Wuhan, China.



Fig. 4 Loading equipment

In the compression tests, the bearing was loaded three times, in which the pressure increased from 0 MPa to the maximum pressure and then decreased to 0 MPa. The effective section area of the bearing was 70686 mm², the vertical design pressure was 10 MPa (SAC, 2006), and the corresponding vertical loading force P_0 was 707 kN. The third load data were analyzed and the vertical stiffness K_v was calculated by

$$K_v = (P_2 - P_1) / (Y_2 - Y_1), \quad (9)$$

where $P_1=0.7P_0$, $P_2=1.3P_0$ are the smaller and larger loading forces, respectively, and Y_1 and Y_2 are the corresponding vertical displacements.

In the compression shear tests, a series of correlation tests on the shear properties were designed to examine the influence of different conditions. In the shear strain correlation tests, the vertical pressure of 5 MPa was applied linearly and kept constant until the

end of the tests. Sinusoidal shear displacements with the peak values of 30, 50, 80, 100, and 120 mm were applied respectively to the bottom connection plate. In the compression pressure correlation tests, the vertical pressures were 2.8, 5, 10, and 12 MPa, respectively, and the peak value of the shear displacement was 50 mm. The loading frequency of all the shear displacements was 0.1 Hz.

5 Numerical simulation and analysis of results

5.1 Numerical simulation

Based on the FE model of the SLRB, numerical simulations of the compression and compression shear tests discussed above have been conducted. To accurately simulate the boundary condition of the bearing, the displacements along the x - and y -directions of the top and side surfaces of the loading plate, as well as the displacements along the y - and z -directions of the bottom connection plate, were constrained for all the tests. It is necessary to point out that all materials in the FE model are rate-independent, which was also made in other research (Ali and Abdel-Ghaffar, 1995; Doudoumis *et al.*, 2005; Weisman and Warn, 2012; Ohsaki *et al.*, 2015), meaning that the rate-dependent effect of materials is neglected in this study. Besides, the computational cost of the explicit analysis is directly relevant to the load duration (Hallquist, 2014). Therefore, the experimental loading frequency of 0.1 Hz was modified to be 1 Hz in numerical simulations to reduce the runtime of the explicit analyses by about 90% without causing theoretical errors.

5.2 Compression test

According to the loading procedure of the experiment, vertical forces of $0.7P_0$ and $1.3P_0$ were applied on the top surface of the loading plate, and the distribution of the vertical displacement is shown in Fig. 5. The vertical displacement is larger along the $+z$ -axis with the largest displacements being 0.556 mm (Fig. 5a) and 1.068 mm (Fig. 5b), from which the vertical stiffness of the SLRB can be calculated as follows:

$$K_v = \frac{(1.3 - 0.7) \times 707}{1.068 - 0.556} \text{ kN/mm} = 828.5 \text{ kN/mm.} \quad (10)$$

The percentage error between the numerical result 828.5 kN/mm and the experimental result 862 kN/mm (Xing *et al.*, 2012) is 3.9%. In the numerical simulation, it is observed that K_v is affected directly by the Poisson's ratio of rubber. In this study, the Poisson's ratio of rubber was 0.4999, and the corresponding bulk modulus of rubber was

$$K = \frac{E}{3(1 - 2\mu)} \approx \frac{G}{(1 - 2\mu)} \quad (11)$$

$$= \frac{0.392 \text{ MPa}}{1 - 2 \times 0.4999} = 1.96 \text{ GPa,}$$

which is consistent with existing findings on the bulk modulus of rubbers (Constantinou *et al.*, 1992).

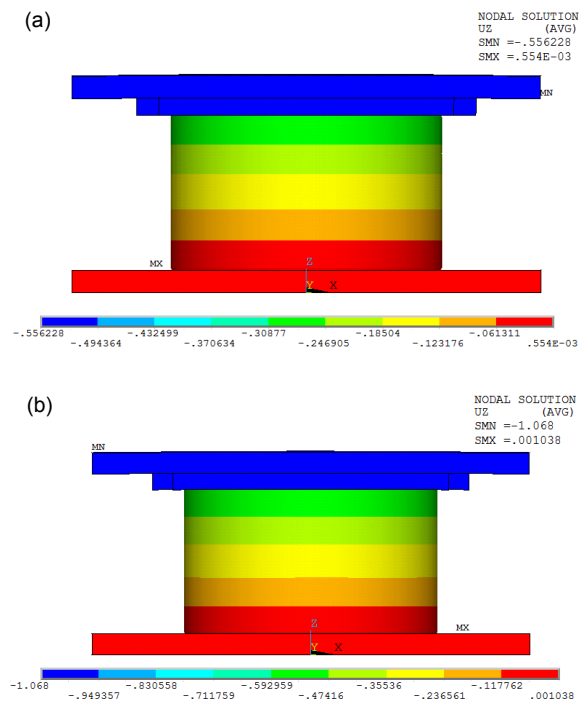


Fig. 5 Vertical displacement (mm) of the sliding lead rubber bearing model: $0.7P_0$ (a) and $1.3P_0$ (b)

5.3 Compression-shear test

5.3.1 Compression

1. Rubber layer

Fig. 6 illustrates the first principal stress of the intermediate rubber layer under a vertical pressure of 5 MPa. It is observed that the first principal stress ranges from -4.934 MPa to -3.238 MPa. The second

and third principal stress distributions of the intermediate rubber layer are almost the same as the first one and they are not shown here. These results indicate that the laminated rubber layers are in a tri-axial compression state, and this is the reason for the large vertical stiffness of bearings.

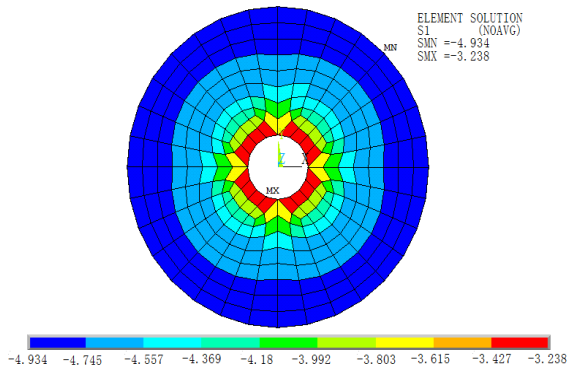


Fig. 6 First principal stress of the intermediate rubber layer

2. Lead

Fig. 7 shows the stress and strain state of the lead when the vertical pressure of 5 MPa was applied to the bearing. Obviously, the lead is bulging outward with the largest displacement along the *x*-axis of 0.011 mm. The largest von Mises stress within the lead is 13.85 MPa. It should be noted that both ends of the lead have already undergone plastic deformation even if no additional lateral load was applied, and the effective plastic strain was defined by

$$\bar{\epsilon}^{pl} = \int_0^t \sqrt{\frac{2}{3} (\dot{\epsilon}^{pl})^T (\dot{\epsilon}^{pl})} dt, \quad (12)$$

where $\dot{\epsilon}^{pl}$ is the effective plastic strain rate (Hallquist, 2014) and the maximum value of Eq. (12) is 1.8×10^{-4} .

5.3.2 Compression shear

1. Comparison of hysteresis curves

(1) Shear strain correlation

Due to the inaccuracy of the test facilities, the actual peak values of the shear displacement were 29, 48, 77, 95, and 115 mm, respectively, which are all somewhat smaller than the design values. Fig. 8 shows the hysteresis curves of the SLRB. It indicates that both the experimental result and the numerical result show the particular ‘slide-isolation’ property as

introduced in Section 2. Thus, the modeling method for the SLRB in this study is capable of reproducing the hysteresis properties of the SLRB very well, including the pre-yield stiffness, post-yield stiffness, sliding force, and maximum restoring force, which demonstrates the accuracy of the developed FE model of the SLRB. However, there still exist some errors in the unloading yield shear force, which result mainly from all the modifications of the SLRB model and the assumptions of material models, including ideal elastoplastic model for lead and the Mooney-Rivlin

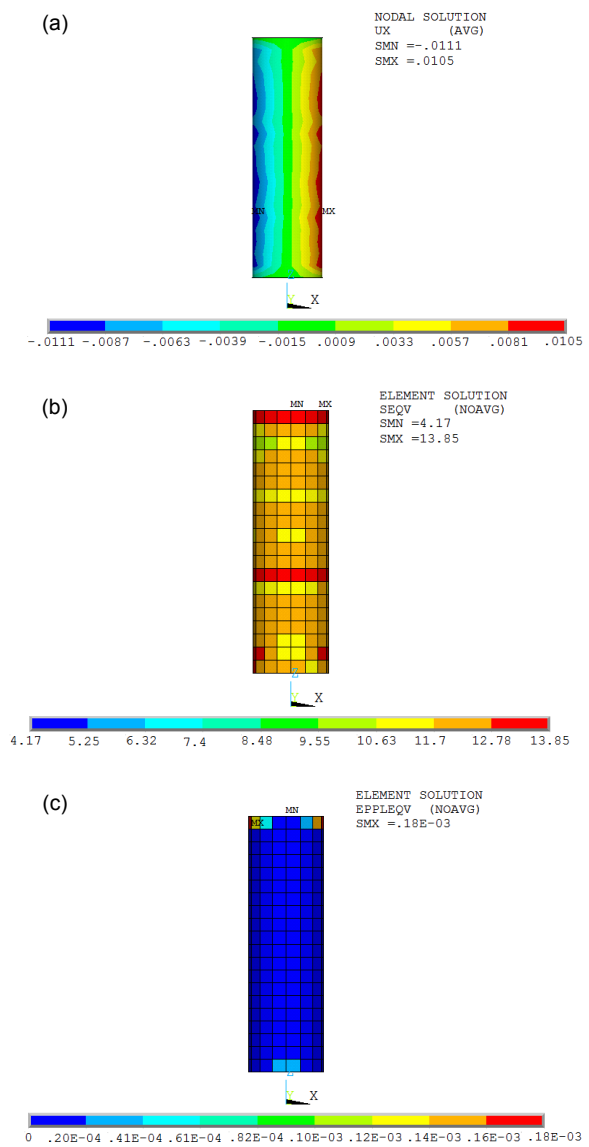


Fig. 7 States of the lead at the vertical pressure of 5 MPa (a) Displacement (mm) along *x*-axis; (b) von Mises stress (MPa); (c) Effective plastic strain

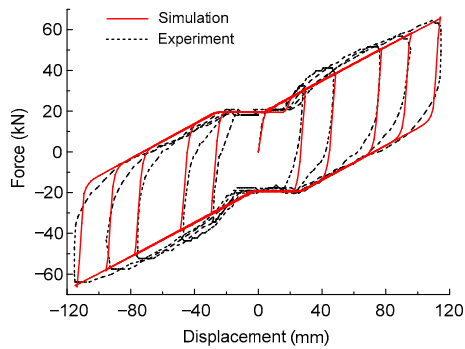


Fig. 8 Hysteresis curves with different shear strains

model for rubber, and both of them are set as rate-independent.

(2) Vertical pressure correlation

After applying the shear displacement of 50 mm under different vertical pressures (2.8, 5, 10, and 12 MPa) to the bearing, the comparison of hysteresis curves from experiment with those from simulation is illustrated in Fig. 9. It is noted that the vertical pressure has a relatively large effect on the hysteresis curve of the SLRB. In Figs. 9a and 9b, both experimental and numerical results indicate that the working principal of the SLRB is ‘slide-isolation’. However, as shown in Fig. 9c, with the increase of vertical pressure, the working principal changes from ‘slide-isolation’ to ‘isolation-slide’, which means that the upper sliding device and the lower LRB first act as a seismic isolation entirety and then the upper device begins to slide when the shear force is larger than the maximum static force. After the friction force has exceeded the largest restoring force of LRB under the vertical pressure of 12 MPa, the upper sliding device loses functionality and the hysteresis curve can characterize only the shear performance of the lower LRB (Fig. 9d). In sum, hysteresis curves from numerical simulation are consistent with the experimental ones.

2. Comparison of the deformed shapes

Fig. 10 shows the deformation of the SLRB in experiment and numerical simulation. In Fig. 10a, the top plate of the bearing is fixed, and the bottom plate is dragged by the compression shear test machine along one direction without undesired rotation. The laminated rubbers undergo obvious large shear deformation. It is noted that the deformed shapes in the numerical simulation are very consistent with those in

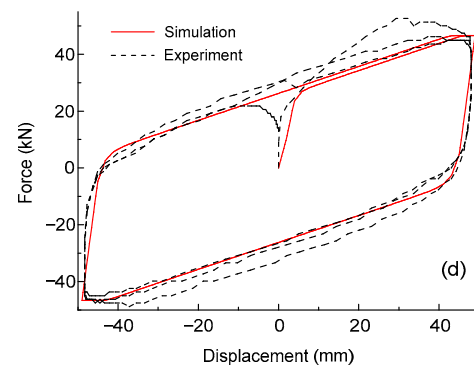
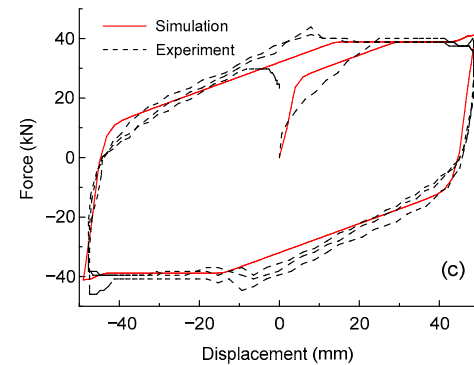
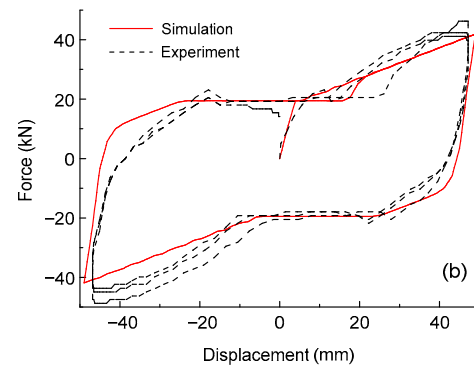
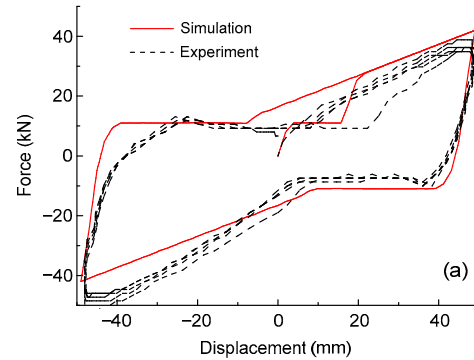


Fig. 9 Hysteresis curves at different vertical pressures (a) 2.8 MPa; (b) 5 MPa; (c) 10 MPa; (d) 12 MPa

experiment. In addition, as illustrated in Fig. 10b, the laminated steels generate almost no shear displacement even if their thickness has been magnified several times. In other words, changing the thickness of the laminated steels has almost no influence on the distribution of shear displacement.

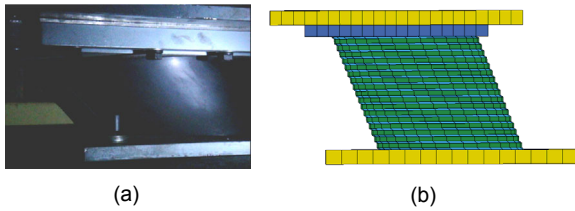


Fig. 10 Deformed shapes of the sliding lead rubber bearing: experiment (a) and numerical simulation (b)

3. Verification of shear stress

To assess the accuracy of the stress states, the shear stresses of the intermediate rubber layer at the shear displacements of 29, 48, 77, 95, and 115 mm are compared with the theoretical results respectively (Table 2).

In Table 2, the shear strain γ , the theoretical shear stress τ , and the error Ω are decided respectively by Eqs. (13)–(15):

$$\gamma = \frac{D - I}{H_r}, \quad (13)$$

$$\tau = G\gamma, \quad (14)$$

$$\Omega = \frac{\sigma_{zx} - \tau}{\tau}, \quad (15)$$

where D is the shear displacement of the bearing, I ($I=15$ mm in this study) is the interval between the baffle and the upper fixing plate, H_r is the total thickness of the rubbers, G represents the shear modulus, and σ_{zx} is the shear stress of the rubbers obtained from numerical simulations. Taking the shear displacements of 48 and 115 mm as examples,

the shear stress distribution of the intermediate rubber layer is plotted in Fig. 11. For simplicity, σ_{zx} is determined by picking the most widespread value. As circled in Fig. 11, it is 0.2114 MPa for 48 mm and 0.6284 MPa for 115 mm.

As listed in Table 2, the errors between the theoretical and numerical results are very small and the largest one is 2.18%, which again verifies the accuracy of the modeling method of the SLRB.

4. State of the lead

Fig. 12 shows the deformed shape of the lead core, as well as the distribution of the von Mises stress and plastic strain, subjected to the maximum shear displacement of 115 mm and vertical pressure of 5 MPa. In Fig. 12a, a significant stretching of the lead is observed, not only in shear but also in elongation. From the distribution of the von Mises stress, the stress has reached the yielding stress of 16 MPa over the whole height of the core. Moreover, the lead core has undergone a large plastic deformation with the minimum and maximum effective plastic strains being 1.267 and 3.505.

5. Vertical stress state of rubbers

Fig. 13 shows the distribution of vertical stress within rubbers with the shear displacement of 115 mm. It is observed that the largest tensile stress is 2.03 MPa at the left bottom margin and the right top margin of the bearing, even if the compression pressure of 5 MPa is applied. The reason for the largest tensile stress at the right top margin is as follows. As shown in Fig. 14, the top connection plate has been separated from the Teflon plate when the bearing undergoes a large shear displacement. This is because the right bottom part of the bearing pulls its upper part, which is also the reason for the tensile stress showing at the right top margin. Through the analysis of vertical stress state of rubbers, it is proposed that the coherence of the steel-rubber interface should be strong enough to sustain possible tensile stress in practical situations, especially when a major earthquake

Table 2 Comparison of the shear stresses of rubbers

Shear displacement (mm)	Shear strain, γ (%)	Theoretical shear stress, τ (MPa)	Actual shear stress, σ_{zx} (MPa)	Error, Ω (%)
29	22.90	0.08994	0.09007	0.15
48	54.10	0.2120	0.2114	-0.28
77	101.60	0.3983	0.3944	-0.98
95	131.10	0.5139	0.5121	-0.35
115	163.90	0.6424	0.6284	-2.18

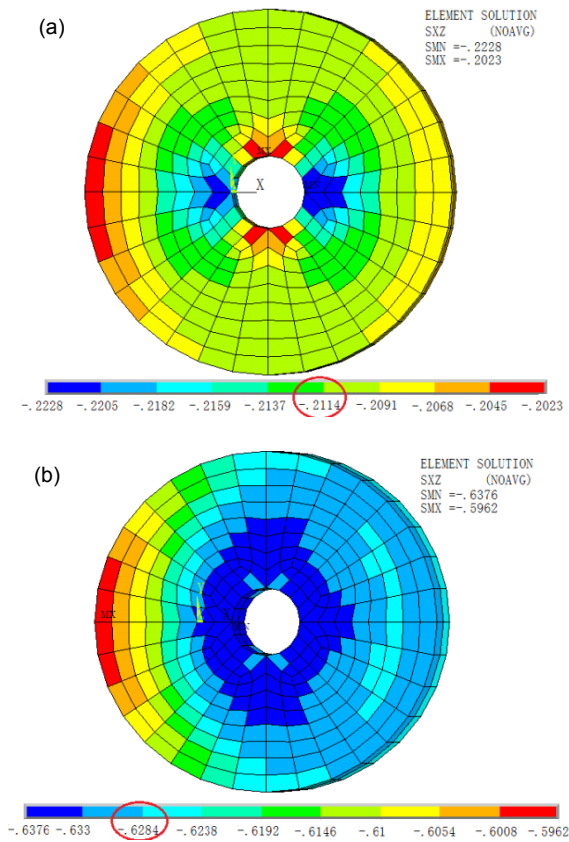


Fig. 11 Shear stresses (MPa) in the intermediate rubber layer
 (a) Shear displacement of 48 mm; (b) Shear displacement of 115 mm

occurs. Besides, more attention should be paid to dust-proofing measures in bearings since the top connection plate may get separated from the Teflon plate.

Finally, it is noteworthy that the elapsed time of the shear correlation test in this study is 266 min. In another study, the same numerical test, conducted by implicit algorithm in ANSYS with the same computer (CPU: Intel Core 3.2 GHz (i5), RAM: 8.0 GB), takes more than two days. Therefore, the modeling method of the SLRB based on the explicit finite program ANASYS/LS-DYNA has better performance in controlling the computational cost of the numerical simulation of bearings.

6 Conclusions

In this paper, the FE model of the SLRB by the explicit FE software ANSYS/LS-DYNA has been

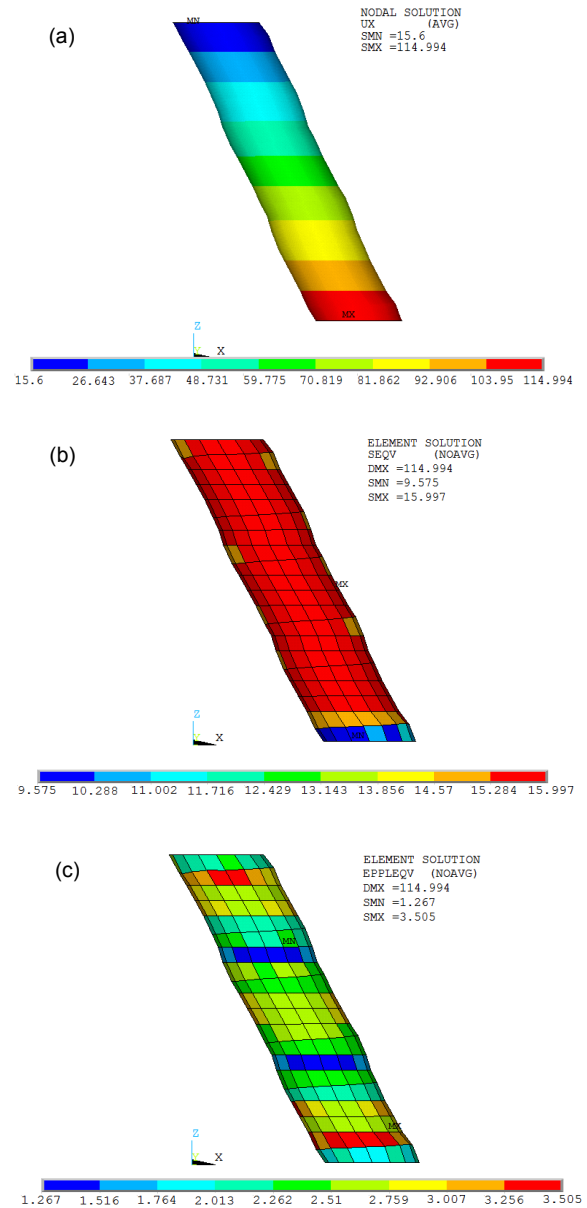


Fig. 12 States of the lead at the shear displacement of 115 mm
 (a) Displacement (mm) along x-axis; (b) von Mises stress (MPa); (c) Effective plastic strain

developed. Numerical simulations of the compression tests and a series of correlation tests on compression-shear properties for the bearing were conducted. Numerical results have been evaluated by both experimental and theoretical studies. Major conclusions are summarized as follows:

1. The time step size, Δt , in each cycle of the SLRB model has been increased from 2.4×10^{-7} s to

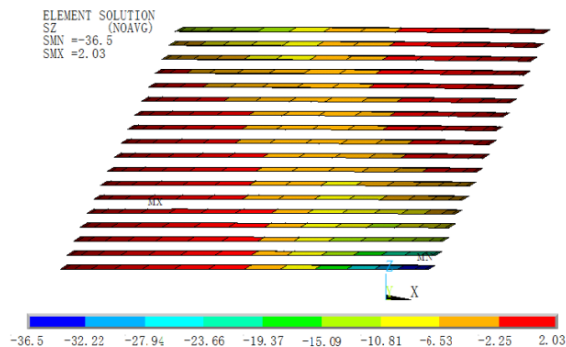


Fig. 13 Vertical stress (MPa) of rubbers

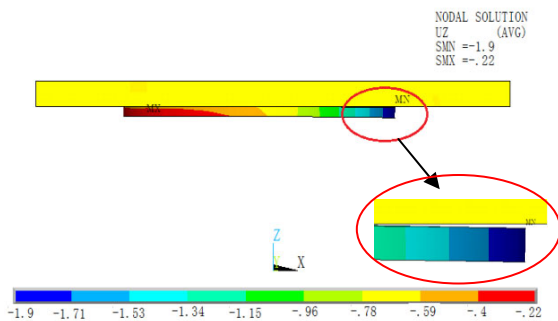


Fig. 14 Vertical displacement (mm) of the SLRB's top part

3.5×10^{-6} s by proper modification of the design parameters of laminated steels, including the density, Young's modulus, and the thickness. These modifications were shown to have only minor influences on the mechanical properties of the bearing.

2. All contact relations existing in the SLRB can be well analyzed by three types of contact relations in ANSYS/LS-DYNA.

3. The modeling method for the SLRB by the explicit FE program is capable of reproducing the vertical stiffness and particular hysteresis behaviors of the SLRB. Besides, the shear stress of the intermediate rubber layer obtained from numerical simulations is very consistent with theoretical results.

4. In the numerical simulation, it is observed that both ends of the lead core have already generated plastic deformation even if no additional lateral load is applied. Moreover, the lead core generated an extremely large plastic deformation when a shear displacement of 115 mm was applied, with the minimum and maximum effective plastic strains being 1.267 and 3.505, respectively.

5. Note that the explicit algorithm runs more efficiently than the implicit algorithm in the numerical simulation of the SLRB.

References

- Abe, M., Yoshida, J., Fujino, Y., 2004a. Multiaxial behaviors of laminated rubber bearings and their modeling. I: Experimental study. *Journal of Structural Engineering*, **130**(8):1119-1132. [http://dx.doi.org/10.1061/\(ASCE\)0733-9445\(2004\)130:8\(1119\)](http://dx.doi.org/10.1061/(ASCE)0733-9445(2004)130:8(1119))
- Abe, M., Yoshida, J., Fujino, Y., 2004b. Multiaxial behaviors of laminated rubber bearings and their modeling. II: Modeling. *Journal of Structural Engineering*, **130**(8):1133-1144. [http://dx.doi.org/10.1061/\(ASCE\)0733-9445\(2004\)130:8\(1133\)](http://dx.doi.org/10.1061/(ASCE)0733-9445(2004)130:8(1133))
- Ali, H.E.M., Abdel-Ghaffar, A.M., 1995. Modeling of rubber and lead passive-control bearings for seismic analysis. *Journal of Structural Engineering*, **121**(7):1134-1144. [http://dx.doi.org/10.1061/\(ASCE\)0733-9445\(1995\)121:7\(1134\)](http://dx.doi.org/10.1061/(ASCE)0733-9445(1995)121:7(1134))
- Amin, A.F.M.S., Alam, M.S., Okui, Y., 2002. An improved hyperelasticity relation in modeling viscoelasticity response of natural and high damping rubbers in compression: experiments, parameter identification and numerical verification. *Mechanics of Materials*, **34**(2):75-95. [http://dx.doi.org/10.1016/S0167-6636\(01\)00102-8](http://dx.doi.org/10.1016/S0167-6636(01)00102-8)
- Amin, A.F.M.S., Wiraguna, S.I., Bhuiyan, A.R., et al., 2006a. Hyperelasticity model for finite element analysis of natural and high damping rubbers in compression and shear. *Journal of Engineering Mechanics*, **132**(1):54-64. [http://dx.doi.org/10.1061/\(ASCE\)0733-9399\(2006\)132:1\(54\)](http://dx.doi.org/10.1061/(ASCE)0733-9399(2006)132:1(54))
- Amin, A.F.M.S., Lion, A., Sekita, S., et al., 2006b. Nonlinear dependence of viscosity in modeling the rate-dependent response of natural and high damping rubbers in compression and shear: experimental identification and numerical verification. *International Journal of Plasticity*, **22**(9):1610-1657. <http://dx.doi.org/10.1016/j.ijplas.2005.09.005>
- Basu, B., Bursi, O.S., Casciati, F., et al., 2014. A European association for the control of structures joint perspective. Recent studies in civil structural control across Europe. *Structural Control and Health Monitoring*, **21**(12):1414-1436. <http://dx.doi.org/10.1002/stc.1652>
- Constantinou, M.C., Kartoum, A., Kelly, J.M., 1992. Analysis of compression of hollow circular elastomeric bearings. *Engineering Structures*, **14**(2):103-111. [http://dx.doi.org/10.1016/0141-0296\(92\)90036-P](http://dx.doi.org/10.1016/0141-0296(92)90036-P)
- de Mari, G., Domaneschi, M., Ismail, M., et al., 2015. Reduced-order coupled bidirectional modeling of the Roll-N-Cage isolator with application to the updated bridge benchmark. *Acta Mechanica*, **226**(10):3533-3553. <http://dx.doi.org/10.1007/s00707-015-1394-3>
- Domaneschi, M., 2012. Simulation of controlled hysteresis by

- the semi-active Bouc-Wen model. *Computers and Structures*, **106-107**:245-257.
<http://dx.doi.org/10.1016/j.compstruc.2012.05.008>
- Doudoumis, I.N., Gravalas, F., Doudoumis, N.I., 2005. Analytical modeling of elastomeric lead-rubber bearings with the use of finite element micromodels. 5th GRACM International Congress on Computational Mechanics.
- Eröz, M., DesRoches, R., 2013. A comparative assessment of sliding and elastomeric seismic isolation in a typical multi-span bridge. *Journal of Earthquake Engineering*, **17(5)**:637-657.
<http://dx.doi.org/10.1080/13632469.2013.771589>
- Gur, S., Mishra, S.K., Chakraborty, S., 2014. Performance assessment of buildings isolated by shape-memory-alloy rubber bearing: comparison with elastomeric bearing under near-fault earthquakes. *Structural Control and Health Monitoring*, **21(4)**:449-465.
<http://dx.doi.org/10.1002/stc.1576>
- Hallquist, J.O., 2014. LS-DYNA Theory Manual. Livermore Software Technology Corporation, California, USA.
- Han, X., Warn, G.P., 2014. Mechanistic model for simulating critical behavior in elastomeric bearings. *Journal of Structural Engineering*, **141(5)**:04014140.
[http://dx.doi.org/10.1061/\(ASCE\)ST.1943-541X.0001084](http://dx.doi.org/10.1061/(ASCE)ST.1943-541X.0001084)
- Hwang, J.S., Chiou, J.M., Sheng, L.H., et al., 1996. A refined model for base-isolated bridge with bi-linear hysteretic bearings. *Earthquake Spectra*, **12(2)**:245-273.
<http://dx.doi.org/10.1193/1.1585879>
- Imbimbo, M., de Luca, A., 1998. F.E. stress analysis of rubber bearings under axial loads. *Computers and Structures*, **68(1-3)**:31-39.
[http://dx.doi.org/10.1016/S0045-7949\(98\)00038-8](http://dx.doi.org/10.1016/S0045-7949(98)00038-8)
- Imbsen, R.A., 2007. AASHTO Guide Specifications for LRFD Seismic Bridge Design. American Association of State Highway and Transportation Officials, USA.
- Kalpakidis, I.V., Constantinou, M.C., Whittaker, A.S., 2010. Modeling strength degradation in lead-rubber bearings under earthquake shaking. *Earthquake Engineering and Structural Dynamics*, **39(13)**:1533-1549.
<http://dx.doi.org/10.1002/eqe.1039>
- Kelly, J.M., Marsico, M.R., 2013. Tension buckling in rubber bearings affected by cavitation. *Engineering Structures*, **56**:656-663.
<http://dx.doi.org/10.1016/j.engstruct.2013.05.051>
- Kelly, J.M., Takhirov, S.M., 2007. Tension buckling in multi-layer elastomeric isolation bearings. *Journal of Mechanics of Materials and Structures*, **2(8)**:1591-1605.
- Medel-Vera, C., Ji, T.J., 2015. Seismic protection technology for nuclear power plants: a systematic review. *Journal of Nuclear Science and Technology*, **52(5)**:607-632.
<http://dx.doi.org/10.1080/00223131.2014.980347>
- Miyamura, T., Yamashita, T., Akiba, H., et al., 2015. Dynamic FE simulation of four-story steel frame modeled by solid elements and its validation using results of full-scale shake-table test. *Earthquake Engineering and Structural Dynamics*, **44(9)**:1449-1469.
<http://dx.doi.org/10.1002/eqe.2526>
- Nguyen, H.H., Tassoulas, J.L., 2010. Directional effects of shear combined with compression on bridge elastomeric bearings. *Journal of Bridge Engineering*, **15(1)**:73-80.
[http://dx.doi.org/10.1061/\(ASCE\)BE.1943-5592.0000034](http://dx.doi.org/10.1061/(ASCE)BE.1943-5592.0000034)
- Ohsaki, M., Miyamura, T., Kohiyama, M., et al., 2009. High-precision finite element analysis of elastoplastic dynamic responses of super-high-rise steel frames. *Earthquake Engineering and Structural Dynamics*, **38(5)**:635-654.
<http://dx.doi.org/10.1002/eqe.900>
- Ohsaki, M., Miyamura, T., Kohiyama, M., et al., 2015. Finite-element analysis of laminated rubber bearing of building frame under seismic excitation. *Earthquake Engineering and Structural Dynamics*, **44(11)**:1881-1898.
<http://dx.doi.org/10.1002/eqe.2570>
- Pan, P., Ye, L.P., Shi, W., et al., 2012. Engineering practice of seismic isolation and energy dissipation structures in China. *Science China Technological Sciences*, **55(11)**:3036-3046.
<http://dx.doi.org/10.1007/s11431-012-4922-6>
- Perotti, F., Domaneschi, M., de Grandis, S., 2013. The numerical computation of seismic fragility of base-isolated nuclear power plants buildings. *Nuclear Engineering and Design*, **262**:189-200.
<http://dx.doi.org/10.1016/j.nucengdes.2013.04.029>
- Roussis, P.C., Constantinou, M.C., Erdik, M., et al., 2003. Assessment of performance of seismic isolation system of Bolu Viaduct. *Journal of Bridge Engineering*, **8(4)**:182-190.
[http://dx.doi.org/10.1061/\(ASCE\)1084-0702\(2003\)8:4\(182\)](http://dx.doi.org/10.1061/(ASCE)1084-0702(2003)8:4(182))
- Ryan, K.L., Kelly, J.M., Chopra, A.K., 2004. Experimental observation of axial load effects in isolation bearings. 13th World Conference on Earthquake Engineering, Paper No. 1707.
- SAC (Standardization Administration of the People's Republic of China), 2006. Rubber Bearings—Part II: Elastomeric Seismic-Protection Isolators for Bridges, GB 20688.2-2006. Standardization Administration of the People's Republic of China (in Chinese).
- Sugita, H., Mahin, S.A., Doboku, K., 1994. Manual for Men-shin Design of Highway Bridges: Ministry of Construction, Japan. Report No. UCB/EERC-94/10, University of California, Berkeley, USA.
- Takayama, M., Tada, H., Tanaka, R., 1992. Finite-element analysis of laminated rubber bearing used in base-isolation system. *Rubber Chemistry and Technology*, **65(1)**:46-62.
<http://dx.doi.org/10.5254/1.3538607>
- Tyler, R.G., Robinson, W.H., 1984. High-strain tests on lead-rubber bearings for earthquake loadings. *Bulletin of the New Zealand National Society Earthquake Engineering*, **17(2)**:90-105.
- Wang, R.Z., Chen, S.K., Liu, K.Y., et al., 2014. Analytical simulations of the steel-laminated elastomeric bridge bearing. *Journal of Mechanics*, **30(4)**:373-382.
<http://dx.doi.org/10.1017/jmech.2014.24>

- Warn, G.P., Ryan, K.L., 2012. A review of seismic isolation buildings: historical development and research needs. *Buildings*, **2**(3):300-325.
<http://dx.doi.org/10.3390/buildings2030300>
- Warn, G.P., Whittaker, A.S., Constantinou, M.C., 2007. Vertical stiffness of elastomeric and lead-rubber seismic isolation bearings. *Journal of Structural Engineering*, **133**(9): 1227-1236.
[http://dx.doi.org/10.1061/\(ASCE\)0733-9445\(2007\)133:9\(1227\)](http://dx.doi.org/10.1061/(ASCE)0733-9445(2007)133:9(1227))
- Weisman, J., Warn, G.P., 2012. Stability of elastomeric and lead-rubber seismic isolation bearings. *Journal of Structural Engineering*, **138**(2):215-223.
[http://dx.doi.org/10.1061/\(ASCE\)ST.1943-541X.0000459](http://dx.doi.org/10.1061/(ASCE)ST.1943-541X.0000459)
- Xing, C.X., Wang, H., Li, A.Q., et al., 2012. Design and experimental verification of a new multi-functional bridge seismic isolation bearing. *Journal of Zhejiang University-SCIENCE A (Applied Physics & Engineering)*, **13**(12): 904-914.
<http://dx.doi.org/10.1631/jzus.A1200106>
- Yoshida, J., Abe, M., Fujino, Y., et al., 2004. Three-dimensional finite-element analysis of high damping rubber bearings. *Journal of Engineering Mechanics*, **130**(5):607-620.
[http://dx.doi.org/10.1061/\(ASCE\)0733-9399\(2004\)130:5\(607\)](http://dx.doi.org/10.1061/(ASCE)0733-9399(2004)130:5(607))

中文概要

题目：一种可滑移式铅芯橡胶支座的显式数值模拟与试验验证

目的：随着隔震技术在工程结构中的逐步推广应用，橡胶隔震支座的试验与数值模拟都得到国内外工程研究人员的重视。其中后者因支座大变形时计

算较难收敛、铅芯与周边橡胶以及钢板的复杂接触关系较难模拟、采用隐式积分算法时计算规模较难控制等问题，目前仍是这一方向的研究热点。本文旨在探讨基于显式积分算法对一种新型可滑移式铅芯橡胶支座进行准确可行的数值模拟的方法。

创新点：1. 探究基于显式积分算法的隔震支座数值模拟方法；2. 采取多种方法有效地控制了数值模拟计算规模，同时实现了较高的数值模拟精度；3. 采用程序中提供的3种接触方式较好地模拟了支座中存在的复杂接触关系。

方法：本文主要采用4种方法减小数值模拟计算规模：1. 激活程序内置的质量缩放功能；2. 合理增大支座中对支座竖向刚度与水平剪切性能影响较小的非关键部件——叠层钢板的厚度；3. 合理减小叠层钢板的弹性模量；4. 考虑到支座中所有材料均未考虑材料的率变效应，即加载速率对支座的力学性能没有影响，本文数值模拟中所用加载频率为实际加载频率的10倍。此外，本文采用了一般接触、绑定接触与单边接触模拟支座中不同的接触关系。

结论：1. 显式积分的计算时间步长由 2.4×10^{-7} s 增大到 3.5×10^{-6} s；2. 与试验结果对比验证了本文提出的基于显式积分算法对该新型可滑移式铅芯橡胶支座进行数值模拟的方法的准确实用性；3. 该支座在纯压作用下，部分铅芯发生塑性变形，而在最大剪切位移时，铅芯发生了很大的塑性流动变形；4. 与采用隐式算法对该支座进行数值模拟研究所用时间相比，显式算法所用时间少很多。

关键词：显式算法；可滑移式铅芯支座；计算时间步长；接触关系；试验验证